Cone myoid elongation involves unidirectional microtubule movement mediated by dynein-1

Tylor R. Lewis[a], Mariusz Zareba[b], Brian A. Link[a], and Joseph C. Besharse[a,b,*]
[a]Department of Cell Biology, Neurobiology, and Anatomy and [b]Department of Ophthalmology, Medical College of Wisconsin, Milwaukee, WI 53226

ABSTRACT **Teleosts and amphibians exhibit retinomotor movements, morphological changes in photoreceptors regulated by light and circadian rhythms. Cone myoid elongation occurs during dark adaptation, leading to the positioning of the cone outer segment closer to the retinal pigment epithelium. Although it has been shown that microtubules are essential for cone myoid elongation, the underlying mechanism has not been established. In this work, we generated a transgenic line of zebrafish expressing a photoconvertible form of α-tubulin (tdEOS-tubulin) specifically in cone photoreceptors. Using superresolution structured illumination microscopy in conjunction with both pharmacological and genetic manipulation, we show that cytoplasmic dynein-1, which localizes to the junction between the ellipsoid and myoid, functions to shuttle microtubules from the ellipsoid into the myoid during the course of myoid elongation. We propose a novel model by which stationary complexes of cytoplasmic dynein-1 are responsible for the shuttling of microtubules between the ellipsoid and myoid is the underlying force for the morphological change of myoid elongation.**

Monitoring Editor
Manuel Théry
CEA, Hopital Saint Louis

Received: Aug 23, 2017
Revised: Oct 31, 2017
Accepted: Nov 7, 2017

INTRODUCTION

Rod and cone photoreceptors are sensitive to a smaller dynamic range of light intensity than they are exposed to on a daily basis (Rodieck, 1998). To accommodate dramatic changes in light intensity, two distinct mechanisms appear to have evolved. In mammals and other higher vertebrates, the pupillary response can control the amount of light that reaches the retina (Atchison and Smith, 2006). In contrast, teleosts, which have a fixed pupil, have evolved retinomotor movements that physically alter the position of rod and cone outer segments as a response to varying degrees of light intensity throughout the day (Ali, 1975).

Retinomotor movements are morphological changes that occur in response to light or darkness (Ali, 1975) and in some cases are regulated as circadian rhythms (Welsh and Osborn, 1937). There are three retinomotor movements that occur in the outer retina (Supplemental Figure S1). First, the pigment granules in the retinal pigment epithelium (RPE) extend through apical processes during the light adaptation (LA) and move basally back toward the RPE cell body during dark adaptation (DA). Second, the rod outer segments (OS) are positioned further apically, near the RPE, whereas cone OS are positioned further basally, closer to the external limiting membrane during LA. The apical positioning of the rod OS in light is thought to function in conjunction with the pigment granules to shield the extremely photosensitive rod OS from excessive light during the daytime, whereas the basal positioning of the cone OS better exposes this less photosensitive structure to light. During DA, the cone and rod OS switch locations, positioning the rod OS to better capture light for night vision (Levinson and Burnside, 1981).

The positioning of the rod and cone OS occur through elongation or contraction of the microtubule-concentrated myoid, a region that, along with the ellipsoid, makes up the inner segment (IS) of the photoreceptor (Figure 1A; Warren and Burnside, 1978). In zebrafish, all cone subtypes are fully elongated within 1 h of DA with an increase in IS length of approximately 40 μm. Red-green double cones and blue cones do not contract until after LA, while UV cones

This article was published online ahead of print in MBoC in Press (http://www.molbiolcell.org/cgi/doi/10.1091/mbc.E17-08-0525) on November 15, 2017.
The authors declare that they have no competing interests.
*Address correspondence to: Joseph C. Besharse (jbeshars@mcw.edu).
Abbreviations used: CIS–COS, cone inner segment–cone outer segment; DA, dark adaptation; E, ellipsoid; ELM, external limiting membrane; EMJ, ellipsoid–myoid junction; IS, inner segment; LA, light adaptation; M, myoid; ONL, outer nuclear layer; OS, outer segment; RPE, retinal pigment epithelium; SIM, structured illumination microscopy; SYN, synapse.

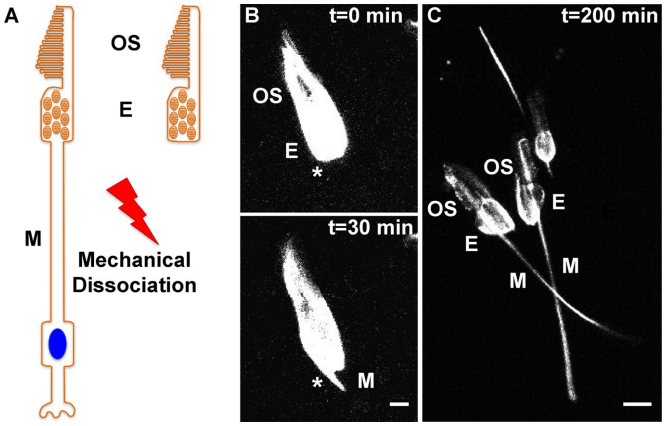

FIGURE 1: CIS–COS are an ex vivo model of myoid elongation. (A) Following DA, cone myoids are fully elongated (Supplemental Figure S1). Retinas can be dissected and mechanically dissociated in medium to generate CIS–COS, which still retain the OS and the mitochondria-concentrated ellipsoid (E). However, the myoid gets broken off during dissociation. (B) Immediately after dissociation in medium, the depicted CIS–COS from a double cone is expressing tdEOS-tubulin and does not contain an observable myoid (top panel). After a short time in culture, the myoid (M) spontaneously elongates from the base of the ellipsoid (*; bottom panel). Scale bar is 5 μm. (C) CIS–COS can be cultured for several hours, during which time they will eventually elongate to the maximal levels observed in vivo. Depicted are three CIS–COS that have undergone dramatic myoid elongation following isolation. Of note, the long myoids are oftentimes bent, such as seen in the top CIS–COS. Scale bar is 10 μm. OS: outer segment; E: ellipsoid; M: myoid; *: ellipsoid–myoid junction.

begin to contract before LA (Menger *et al.*, 2005). Although 75% of double cone contraction occurs within the first 5 min of LA (Hodel *et al.*, 2006), there has been no investigation into exact rates of zebrafish cone elongation during the first hour of DA. Additionally, zebrafish retinomotor movements achieve adult levels by 28 d postfertilization (dpf) (Hodel *et al.*, 2006), providing an excellent system for the use of transgenic and gene editing techniques in studying retinomotor movements.

Original work in the green sunfish has shown that microtubules are essential for cone elongation (Warren and Burnside, 1978), although the mechanism by which microtubules participate has not been determined. Microtubules within the myoid and ellipsoid have the same polarity, with plus ends positioned toward the external limiting membrane and minus ends toward the basal body and accessory centriole (Troutt and Burnside, 1988). It has been proposed that sliding between these microtubules could provide the force for myoid elongation (Warren and Burnside, 1978). Much of this work investigating the mechanism and regulation of myoid elongation has utilized ex vivo preparations of isolated cone inner segments–cone outer segments (CIS–COS; Troutt *et al.*, 1990; Burnside *et al.*, 1993; Hillman *et al.*, 1995; Rey and Burnside, 1999), which break apart at the myoid but still contain the mitochondria-enriched ellipsoid that allows for CIS–COS to perform normal biological functions, such as myoid elongation, for several hours in culture (Figure 1).

In this work, we generated a transgenic line of zebrafish expressing a photoconvertible form of α-tubulin (tdEOS-tubulin; Lu *et al.*, 2013) under control of a cone-specific promoter. Using superresolution structured illumination spectroscopy (SIM) of CIS–COS, we photoconverted and analyzed the movement of the labeled tdEOS-tubulin during myoid elongation. Our data show that myoid elongation is not dependent on new polymerization of microtubules, but rather the movement of polymerized microtubules already concentrated within the ellipsoid. Finally, we show that myoid elongation can be blocked both in vivo and ex vivo by either genetic or pharmacological inhibition of cytoplasmic dynein-1. These observations suggest a model in which preformed microtubules are moved from the ellipsoid into the myoid during elongation.

RESULTS

Ex vivo myoid elongation involves the unidirectional movement of microtubule bundles

In this work, we sought to analyze rates of myoid elongation as well as to study the microtubule-mediated forces that have been proposed as the mechanism of myoid elongation. To answer these questions, we generated a transgenic line of zebrafish expressing α-tubulin tagged with tdEOS, a photoconvertible fluorophore (Lu *et al.*, 2013), under control of the transducin-α cone-specific promoter (TαCP; Kennedy *et al.*, 2007). As previously reported, native tdEOS emits fluorescence at 516 nm (green), but can undergo an irreversible photoconversion via exposure to 405 nm light (UV). The "photoconverted" form of tdEOS emits fluorescence maximally at 582 nm (red; McKinney *et al.*, 2009). Using this ability to photoconvert tdEOS-tubulin, we can monitor the movement within cones of specific subpopulations of microtubules that incorporate tdEOS-tubulin (Lu *et al.*, 2013).

For ease of photoconversion, we initially used ex vivo preparations of CIS–COS that can be imaged with relative ease in conjunction with various drug treatments. When isolated in culture, CIS–COS break apart near the mitochondria-enriched ellipsoid and lack a myoid (Figure 1A). However, over time, CIS–COS exhibit dynamic and dramatic myoid elongations (Figure 1, B and C) that have been used extensively to model in vivo myoid elongation (Troutt *et al.*, 1990; Burnside *et al.*, 1993; Hillman *et al.*, 1995; Rey and Burnside, 1999). With these CIS–COS, we first tested the idea that myoid elongation is a result of microtubule sliding between microtubules within the myoid itself (Figure 2). The cone myoid in vivo typically contains ~20 microtubules (Supplemental Figure S2). Although resolving individual microtubules is below the resolution limit of the SIM, there are definitively multiple microtubules within the myoid as the average fluorescence intensity of tdEOS-tubulin within the myoid is nearly sixfold greater than the fluorescence intensity of what are presumably individual microtubules within the ellipsoid (Supplemental Figure S3). In addition, direct observations of multiple microtubules entering the myoid (Figure 3 and Supplemental Movie S2) further indicate that CIS–COS myoids contain multiple microtubules.

Through photoconversion, we labeled two ~1–2 μm "spots" of tdEOS-tubulin–labeled microtubules within the myoid (Figure 2 and Supplemental Movie S1). During myoid elongation, we observed that all of these tdEOS-tubulin–labeled microtubules within the myoid appeared to be moving together (Figure 2 and Supplemental Movie S1), suggesting that microtubule sliding was not occurring between these microtubules within the myoid. Additionally, we observed that tdEOS-tubulin–labeled microtubules within the ellipsoid appear to be shuttled into the narrow myoid throughout the entire time course of myoid elongation. To further test this observation, we photoconverted two "spots" of tdEOS-tubulin–labeled microtubules within the ellipsoid and monitored their movement during myoid elongation (Figure 3 and Supplemental Movie S2). Indeed, these preformed microtubules within the ellipsoid were shuttled out into the myoid at a rate consistent with the overall rate of myoid elongation. To definitively rule out the possibility of microtubule

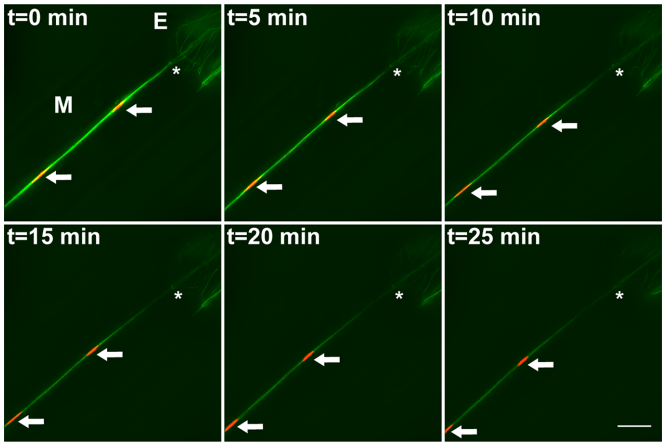

FIGURE 2: Microtubules within the myoid move in unison during ex vivo myoid elongation. Focal photoconversion of two subpopulations of tdEOS-tubulin–labeled microtubules (arrows) within the myoid (M) during a period of extensive myoid elongation of an isolated CIS–COS reveals a concerted and unidirectional movement of microtubules within the myoid (Supplemental Figure S2). Of note, both the "spot length" of each photoconverted spot and the distance between the two photoconverted spots remain unchanged over time, while the distance between the proximal photoconverted spot and the EMJ (*) increases over time. Images are collected at 5-min intervals over the course of 25 min. Additionally, the green tdEOS-tubulin signal appears to photobleach slightly faster than the red tdEOS-tubulin signal. Scale bar is 5 μm. M: myoid; E: ellipsoid; *: ellipsoid–myoid junction. See also Supplemental Movie S1.

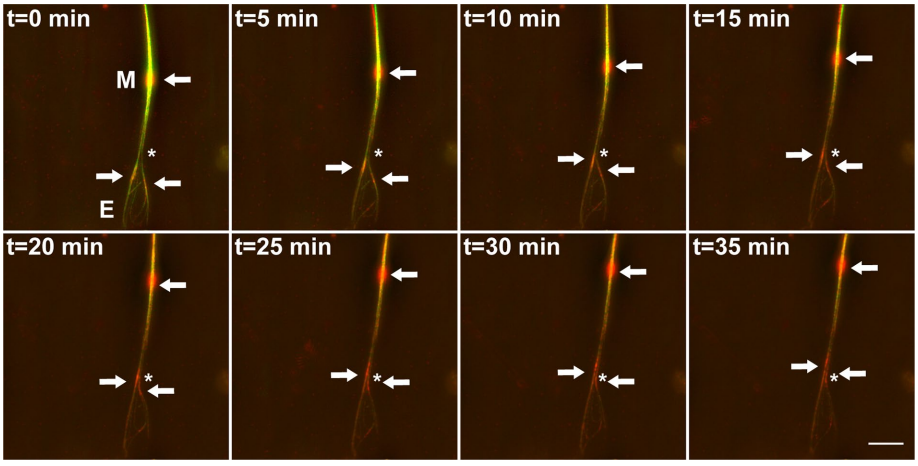

FIGURE 3: Microtubules are shuttled from the ellipsoid to the myoid during ex vivo myoid elongation. Focal photoconversion of two subpopulations of tdEOS-tubulin–labeled microtubules (lower arrows) within the ellipsoid (E) and one subpopulation (higher arrow) within the myoid (M) during a period of extensive myoid elongation of an isolated CIS–COS reveals a concerted and unidirectional shuttling of ellipsoid microtubules into the myoid. Of note, although the distance between the photoconverted spot in the myoid and the EMJ (*) increases over time, the distance between the photoconverted spot in the myoid and those in the ellipsoid remains unchanged over time. Further, the "spot length" of each photoconverted spot remains unchanged over time. Also of note, outside of the predominant photoconverted spots of tdEOS-tubulin–labeled microtubules that appear to shuttle unidirectionally into the myoid during elongation, there are smaller subpopulations of photoconverted tdEOS-tubulin that remain within the ellipsoid and appear to slide against other microtubules. Thus, although microtubules appear to be bundled within the myoid, there is still evidence of regular microtubule-microtubule sliding within the ellipsoid. Images are collected at 5-min intervals over the course of 35 min. Additionally, the green tdEOS-tubulin signal appears to photobleach slightly faster than the red tdEOS-tubulin signal. Scale bar is 5 μm. M: myoid; E: ellipsoid; *: ellipsoid–myoid junction. See also Supplemental Movie S2.

sliding between microtubules within the myoid as a mechanism of myoid elongation, we quantified the length of each photoconverted ~1–2 μm "spot" of tdEOS-tubulin–labeled microtubules within the myoid throughout 20 min of myoid elongation. If microtubule sliding between the microtubules of the myoid was occurring, we would expect the spot length to dramatically increase over time as the myoid elongates. However, there is very little change in the size of these photoconverted tdEOS-tubulin spots (Figure 4A) suggesting that microtubules within the myoid are indeed moving synchronously as microtubule bundles. Additionally, the distance between adjacent photoconverted spots within the myoid did not change over time. In the example in Figure 2, the interspot distance remained constant at ~16 μm during a period when the myoid elongated ~8 μm as indicated by the distance between the asterisk and the first spot. The average rate of myoid elongation in all experiments was 0.17 ± 0.04 μm/min (Figure 4B).

Because of the uniform polarity of microtubules within the myoid (Troutt and Burnside, 1988), new microtubule polymerization within the myoid would occur mainly at the distal, plus end of the growing myoid. We observe that the "spot" of photoconverted tdEOS-tubulin does not remain stationary but instead moves distally as the myoid elongates (Figure 5A). In fact, the distance between this "spot" of photoconverted tdEOS-tubulin and the distal tip of a growing myoid does not change during the time course of myoid elongation (Figure 5B and Supplemental Movie S3), such that the rate of microtubule movement into the myoid is the same as the overall rate of myoid elongation, implicating these two processes. Additionally, the consistent movement of the "spot" of photoconverted tdEOS-tubulin is not consistent with the idea that new microtubule polymerization at the distal tip of the myoid is the underlying mechanism of myoid elongation. In support of this, we treated isolated CIS–COS with 3.3 μM nocodazole, a drug that inhibits microtubule polymerization. This concentration has previously been used to disrupt microtubule dynamics in zebrafish neurons (Butler *et al.*, 2010), although dramatic effects have been observed in zebrafish treated with doses that are up to 10-fold less (Jesuthasan and Stahle, 1997; Efremov *et al.*, 2007; Butler *et al.*, 2010; Mendieta-Serrano *et al.*, 2013). During this short treatment of CIS–COS with nocodazole, we observed no effect on the frequency of myoid elongation (Figure 4C). In addition, nocodazole treatment had no effect on the photoconverted spot length (Figure 4A) or the overall rate of myoid elongation (Figure 4B), further suggesting that new microtubule polymerization is not the dominant driving force of myoid elongation. Instead, it appears as if already polymerized microtubules from the ellipsoid are shuttled into the myoid during myoid elongation. In support of this, the number of observed microtubule filaments within the ellipsoid of a CIS–COS decreases over 30% during a 25-min time course of myoid elongation (Figure 4D). Taken together, these data imply that the unidirectional movement of microtubules into the myoid occurs during elongation, and that myoid elongation is not exclusively

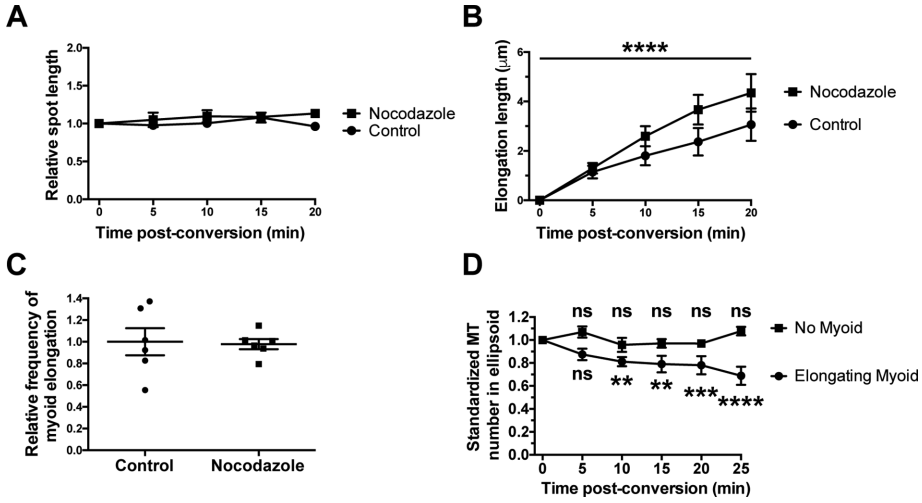

FIGURE 4: Polymerized microtubules from the ellipsoid move into the myoid during elongation. (A) Using focal photoconversion of a 1–2 μm "spot" of tdEOS-tubulin–labeled microtubules tests the prevailing theory that microtubules sliding against one another within the myoid leads to myoid elongation. The size of the photoconverted "spot" of tdEOS-tubulin in the myoid is measured during a 20-min period of myoid elongation for both control ($n = 5$ preparations, 11 total cells imaged) and nocodazole treated ($n = 5$ preparations, nine total cells imaged) CIS–COS. Repeated measures two-way ANOVA reveals no significant changes in spot length over time ($p = 0.3492$) or between treatment conditions ($p = 0.2459$). Data are depicted as mean ± SEM. (B) Rates of myoid elongation can be calculated as the distance that the photoconverted "spot" of tdEOS-tubulin within the myoid travels away from the ellipsoid during 20 min for both control ($n = 5$ preparations, 11 total cells imaged) and nocodazole treated ($n = 5$ preparations, nine total cells imaged) CIS–COS. Repeated measures two-way ANOVA reveals that the myoid significantly elongates over time ($p < 0.0001$, shown) in both the presence and absence of nocodazole. Although those treated with nocodazole actually appear to elongate more, this effect is not significantly different from untreated ($p = 0.2131$). Data are depicted as mean ± SEM. (C) Frequency of myoid elongation in control ($n = 6$ preparations, 1523 total cells counted) or nocodazole treated ($n = 6$ preparations, 1772 total cells counted) is not significantly different as revealed by a two-tailed t test ($p = 0.8726$). Data are depicted as mean ± SEM. (D) The linear microtubule filaments within the ellipsoid were counted during a 25-min period of a CIS–COS that was either undergoing myoid elongation ($n = 5$ preparations, five total cells imaged) or stationary without a myoid ($n = 5$ preparations, five total cells imaged) and standardized to the initial timepoint. Repeated measures two-way ANOVA reveals that there is a significant interaction between the number of microtubules within the ellipsoid over time and the state of myoid elongation ($p = 0.0003$). Bonferroni's multiple comparisons post hoc test reveals no significant differences in the number of microtubules in the ellipsoid of a CIS–COS that is not undergoing myoid elongation at any timepoint compared with the initial timepoint (ns, shown), but significant decreases after 10 min in the number of ellipsoid microtubules in a CIS–COS that is undergoing myoid elongation (shown). Data are depicted as mean ± SEM.

driven by microtubule-microtubule sliding within the myoid or by new microtubule polymerization.

Ex vivo myoid elongation is dependent on cytoplasmic dynein-1

Occasionally during imaging of myoid elongation in CIS–COS, we observed punctate tdEOS-tubulin labeling at the interface between the ellipsoid and myoid or the ellipsoid–myoid junction (EMJ; Figure 2). Because polymerized tdEOS-tubulin–labeled microtubules within the ellipsoid are shuttled out into the myoid during myoid elongation, we hypothesized the existence of a structure around the EMJ involved in this trafficking of polymerized microtubules. Because microtubules within the myoid have uniform polarity with plus ends facing outward and minus ends toward the ellipsoid (Troutt and Burnside, 1988), it is possible that this putative structure around the EMJ could involve anchored cytoplasmic dynein motors. In support of this, cytoplasmic dynein has been previously proposed to be involved in the microtubule sliding model of myoid elongation based on crude pharmacological approaches (Gilson *et al.*, 1986). Indeed, we show that two components of cytoplasmic dynein-1, Dync1H1 and Dync1I2 (Vaughan and Vallee, 1995), appear to localize to the EMJ (Figure 6, A and B). In addition, dynein intermediate chains also specifically localize to the base of the ellipsoid in isolated CIS–COS (Supplemental Figure S4), implying that cytoplasmic dynein-1 could be functioning in myoid elongation in CIS–COS. To further test our hypothesis, we treated isolated CIS–COS with ciliobrevin D, a cytoplasmic dynein-specific inhibitor (Firestone *et al.*, 2012), at a range of concentrations between 10 and 25 μM (Figure 6C). At low doses, we saw no inhibition of myoid elongation in isolated CIS–COS, but at 20 μM and above, there was a significant decrease in myoid elongation, suggesting that one of the two cytoplasmic dynein complexes is required for proper myoid elongation. To validate that the observed effect on inhibition of myoid elongation by ciliobrevin D was a specific and reversible inhibition of cytoplasmic dynein-1, we treated CIS–COS with 20 μM ciliobrevin D and then washed out the drug after 1 h (Figure 6D). Before the wash, myoid elongation was significantly inhibited by ciliobrevin D treatment. Following washing the drug out, myoids began to elongate and reached control levels.

To test the requirement for cytoplasmic dynein-1 genetically, we used *cnb* fish, a line with a nonsense mutation in *dync1h1*, the cytoplasmic dynein-1 heavy chain (Insinna *et al.*, 2010). Because these homozygous mutants die between 6 and 8 dpf, we used adult heterozygotes that were expressing TαCP:tdEOS-tubulin and compared them to wild-type siblings with regard to the frequency of myoid elongation of ex vivo CIS–COS (Figure 6E). In agreement with our pharmacological approach, a heterozygous genetic lesion in *dync1h1* also significantly reduced the frequency of myoid elongation.

In vivo myoid elongation is dependent on cytoplasmic dynein-1

Previous work has shown that, within 1 h of DA, all zebrafish cone subtypes are maximally elongated in vivo (Menger *et al.*, 2005). Although our previous experimentation relied on imaging CIS–COS ex vivo, we sought to use the TαCP:tdEOS-tubulin fish to both analyze the specific rates of myoid elongation during this initial period of DA and investigate the role of cytoplasmic dynein-1 in this process in vivo. We first collected adult wild-type zebrafish that were expressing TαCP:tdEOS-tubulin at five discrete timepoints during 90 min of DA and imaged the tdEOS-tubulin–labeled cytoskeleton of cones (Figure 7A). Of note, the fully contracted, light-adapted cones

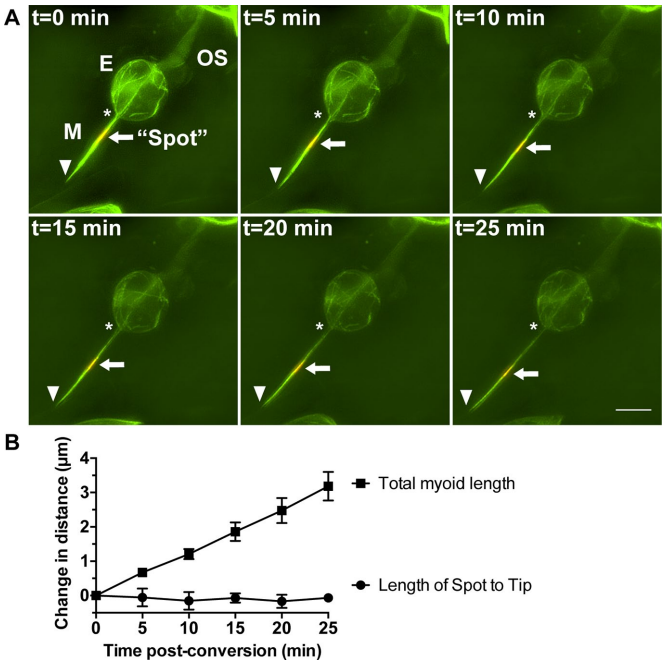

FIGURE 5: Unidirectional microtubule movement rates are consistent with the rates of myoid elongation. (A) Focal photoconversion of a "spot" of tdEOS-tubulin–labeled microtubules (arrow) within the myoid (M) during a period of extensive myoid elongation of an isolated CIS–COS reveals a concerted and unidirectional movement of the myoid microtubules that is in unison with the distal tip of the elongating myoid (arrowhead). Images are collected at 5-min intervals over the course of 25 min. Scale bar is 5 μm. M: myoid; E: ellipsoid; OS: outer segment; *: ellipsoid–myoid junction. See also Supplemental Movie S3. (B) The distance between the photoconverted "spot" of tdEOS-tubulin and the distal tip of the growing myoid is measured and compared with the total length of the myoid during a time period of elongation. The distance between the "spot" and the distal tip of the myoid does not change over time, suggesting that the overall rate of myoid elongation is consistent with the rate of unidirectional microtubule movement within the myoid. Repeated measures two-way ANOVA reveals that there is a significant difference between the change in distance of the "spot" to the distal tip of the myoid over time and the change in the length of the myoid ($p < 0.0001$). Bonferroni's multiple comparisons post hoc test reveals no significant change in the distance between the photoconverted "spot" of tdEOS-tubulin to the distal tip of the myoid at any timepoint compared with the initial timepoint (ns). Data are depicted as mean ± SEM.

contain a strong concentration of tdEOS-tubulin at the EMJ, further supporting our model that polymerized microtubules provide the mechanistic forces for myoid elongation. During DA, the cones readily elongate at a steady rate, while the concentrated tdEOS-tubulin signal decreases. Using line intensity analysis of the tdEOS-tubulin signal, we could track both rates of myoid elongation and total tdEOS-tubulin within the IS over 90 min of DA (Figure 7B). A peak of tdEOS-tubulin signal is observed in the synapse as well as a peak associated with the adherens junctions of the external limiting membrane, which can be validated by immunofluorescence (Supplemental Figure S5), and defines the width of the outer nuclear layer (ONL). As expected, this ONL measurement did not significantly change during DA. tdEOS-tubulin also labels the region around the basal body (Supplemental Figure S6), or the base of the connecting cilium, and can be used to measure the length of the entire IS (including myoid and ellipsoid), or the distance between the external limiting membrane and connecting cilium. In contrast to the constant ONL length through DA, the IS length of wild-type cones continually increases during DA as expected.

From the line intensity analysis, we could then compare the overall elongation of the IS with the total tdEOS-tubulin signal intensity within the IS consisting of both the ellipsoid and myoid (Figure 7C). Through 90 min of DA, the intensity of the tdEOS-tubulin signal in the IS increased only ~50%, suggesting a small level of microtubule influx into the IS during myoid elongation. However, during this same period, relative IS elongation increased ~150%. This significant threefold difference in IS elongation compared with microtubule influx suggests that polymerized microtubules that are already within the IS, such as those seen at the EMJ (Figure 7A), must be directly involved in myoid elongation.

We subsequently collected adult wild-type and *dync1h1* heterozygous siblings expressing TαCP:tdEOS-tubulin during 90 min of DA to quantify rates of myoid elongation (Figure 7D). IS elongation of wild-type fish occurred at a rate of 0.5 ± 0.1 μm/min for the first hour, significantly faster than that of *dync1h1* heterozygotes at 0.2 ± 0.1 μm/min. Taken together, these data strongly implicate cytoplasmic dynein-1 as the force-generating motor leading to microtubule shuttling during myoid elongation.

DISCUSSION

Because of the stark transition of morphology between the wide, rounded ellipsoid and the narrow myoid, we were interested in a cytoskeletal complex at this EMJ that could potentially be involved in maintaining this constricted morphology. Owing to our observation of polymerized microtubules moving from the ellipsoid to myoid during myoid elongation, we hypothesized that a complex around the EMJ likely included microtubule motors that could provide the forces required for microtubule movement. In this work, we identify components of cytoplasmic dynein-1 localized to the EMJ and describe the dependence of cytoplasmic dynein-1 in cone myoid elongation. As a retrograde motor, dynein-1 traffics toward the minus ends of microtubules. With the uniform polarity of microtubules within the myoid, where the plus ends are pointed toward the nucleus and the minus ends are toward the ellipsoid, stationary dynein-1 around the EMJ could function to shuttle microtubules from the ellipsoid into the myoid during myoid elongation. Additionally, dynein-1 could be involved in maintaining the uniform polarity of microtubules within the myoid, similar to its function in polarity-sorting transport of microtubules during axon outgrowth (del Castillo *et al.*, 2015; Rao *et al.*, 2017). Interestingly, comparable complexes of stationary cytoplasmic dynein-1 that are anchored to the actin cortex are responsible for the uniform polarity of microtubules during axon outgrowth (del Castillo *et al.*, 2015). Of note, we frequently observed a close association of tdEOS-tubulin–labeled microtubules in the ellipsoid of CIS–COS with the actin network, particularly at the base of the ellipsoid (Supplemental Figure S7A). Indeed, myoid elongation is reversibly inhibited by depolymerizing the actin cytoskeleton with 10 μM latrunculin B (Supplemental Figure S7B), implying that the actin cytoskeleton is essential for cone myoid elongation. Ultimately, we propose that stationary cytoplasmic dynein-1 complexes anchored to cortical actin around the base of the ellipsoid function to shuttle microtubules into the myoid from the ellipsoid during cone myoid elongation (Figure 8). However, how these stationary cytoplasmic dynein-1 complexes specifically localize to cortical actin at the base of the ellipsoid in contrast to the rest of the cell cortex remains unknown.

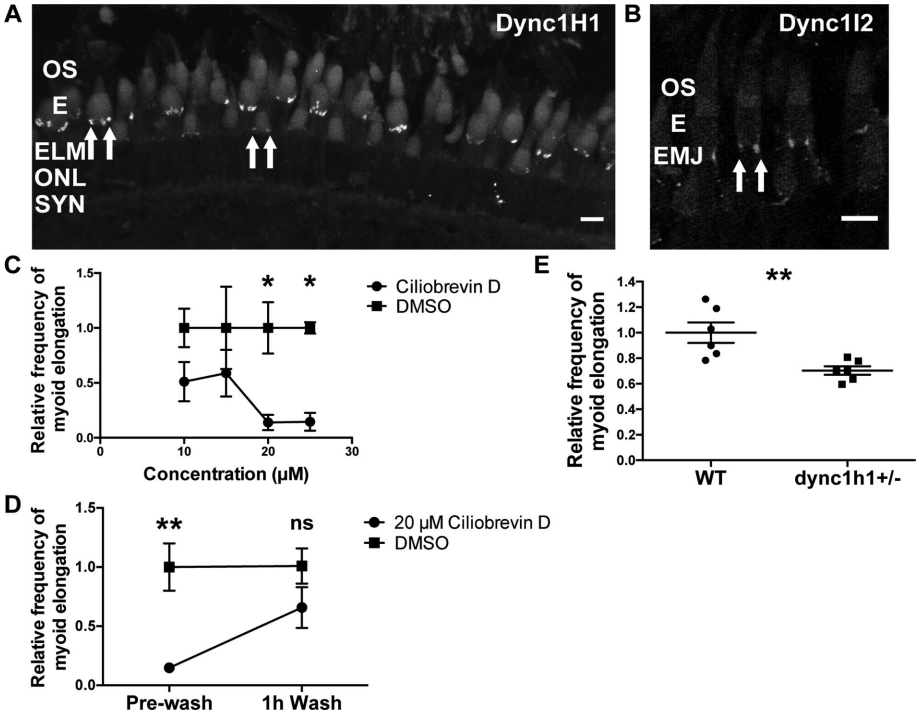

FIGURE 6: Cytoplasmic dynein-1 localizes to the ellipsoid–myoid junction and is required for *ex vivo* myoid elongation. (A) Immunofluorescence staining for Dync1H1, the cytoplasmic dynein-1 heavy chain, reveals localization of discrete puncta at the ellipsoid–myoid junction (EMJ) of cones. The zebrafish retina is tiered with different layers of cone photoreceptors, and Dync1H1 localization around the EMJ appears significantly more intense for the distal cones than for the proximal cones. Scale bar is 10 μm. (B) Immunofluorescence staining for Dync1I2 (Vaughan and Vallee, 1995), an intermediate chain of cytoplasmic dynein-1, reveals a similar localization of discrete puncta around the EMJ. However, the staining intensity is decreased compared with Dync1H1. Scale bar is 10 μm. (C) Frequency of myoid elongation is quantified in CIS–COS treated with either control 0.025% DMSO ($n = 3$ preparations in each of four experiments, 2792 total cells) or 10–25 μM ciliobrevin D treatment, a cytoplasmic dynein-specific inhibitor, at doses between 10 and 25 μM ($n = 3$ preparations at each dose, 2461 total cells). Two-way ANOVA reveals a significant effect of ciliobrevin D treatment ($p = 0.0003$). Bonferroni's multiple comparisons post hoc test reveals a significant decrease in myoid elongation at both 20 μM ($p = 0.0305$) and 25 μM ($p = 0.0319$) of ciliobrevin D. Data are depicted as mean ± SEM. (D) Frequency of myoid elongation is quantified in CIS–COS treated with either control 0.025% DMSO ($n = 5$ preparations, 711 total cells) or 20 μM ciliobrevin D treatment ($n = 5$ preparations, 545 total cells). After initial imaging, CIS–COS were washed with an excess of L10 medium and imaged after 1 h for both control CIS–COS (374 total cells) or ciliobrevin D–washed CIS–COS (266 total cells). Two-way ANOVA reveals a significant effect of ciliobrevin D treatment ($p = 0.0012$). Bonferroni's multiple comparisons post hoc test reveals a significant decrease in frequency of myoid elongation prewash ($p = 0.0024$, shown) but not after washing ($p = 0.2516$, shown). Data are depicted as mean ± SEM. (E) Frequency of myoid elongation is quantified in CIS–COS isolated from either wild-type ($n = 6$ fish, 1985 total cells) or *dync1h1*+/– ($n = 6$ fish, 2120 total cells) adult zebrafish. Two-tailed *t* test reveals a significant decrease in myoid elongation frequency of *dync1h1*+/– zebrafish ($p = 0.0063$). Data are depicted as mean ± SEM.

Alternatively, there are other possible models by which cytoplasmic dynein-1 complexes could be stationary around the EMJ. First, dynein-1 could be anchored to the plasma membrane through some other putative complex. Importantly, these complexes must not create a barrier for plasma membrane dynamics around the EMJ because myoid elongation requires expansion of the myoid plasma membrane. Along with transport of microtubules into the myoid, the myoid plasma membrane must also be expanded either from the ellipsoid plasma membrane or from cytoplasmic vesicular pools in the IS. Second, the cytoplasmic dynein-1 complex around the EMJ could be anchored to a part of a larger cytoskeletal complex rather than tethered to the plasma membrane. In photoreceptors, the ciliary rootlet is a long, filamentous cytoskeletal structure that extends from the basal body through myoid (Spira and Milman, 1979) that is believed to function as a support structure for the OS (Yang *et al.*, 2005). Typically associated with the nuclear envelope, Nesprin1 has recently been shown to interact with ciliary rootlets (Potter *et al.*, 2017), and is known to complex with cytoplasmic dynein-1 during nuclear migration (Zhang *et al.*, 2009). Thus, another potential model is that the ciliary rootlet or another cytoskeletal structure anchors cytoplasmic dynein-1 around the EMJ, allowing for microtubule shuttling during myoid elongation. Because of the lack of direct association of the cytoplasmic dynein-1 complex with the plasma membrane in this model, plasma membrane would be able to freely diffuse into the myoid during the elongation of this compartment. Future work investigating genetic interactions in cone myoid elongation between *dync1h1* and other cytoskeletal genes will assist in identifying other components associated with this complex around the EMJ.

Although much of the early work investigating retinomotor movements has focused on cytoskeletal regulation (Burnside, 1978; Warren and Burnside, 1978), there is also a rich body of work on light and circadian regulation of these processes (Burnside *et al.*, 1993, 2001; Menger *et al.*, 2005). Several studies have shown the involvement of cAMP in promoting dark-adapted retinomotor movements, including cone myoid elongation (Besharse *et al.*, 1982; Gilson *et al.*, 1986; Rey and Burnside, 1999). It has been proposed that protein kinase A (PKA), the cAMP-dependent kinase (Taylor, 1989), is involved in the regulation of cytoskeletal-dependent retinomotor movements (Gilson *et al.*, 1986), and has since been shown to regulate rod myoid elongation (Liepe and Burnside, 1993). Although there have been investigations of potential downstream targets of PKA in the retinomotor movement pathway (Pagh-Roehl *et al.*, 1993, 1995), PKA has recently been shown to directly regulate cytoplasmic dynein-1 in binding lysosomes and viral particles (Scherer *et al.*, 2014). Thus, one promising avenue of future work will involve investigating whether the light and circadian regulation of cone myoid elongation converges on the regulation of this cytoplasmic dynein-1 complex around the EMJ through phosphorylation by PKA.

A vast amount of work on the mechanisms and regulation of myoid elongation has been performed on preparations of CIS–COS (Troutt *et al.*, 1990; Burnside *et al.*, 1993; Hillman *et al.*, 1995; Rey and Burnside, 1999), although there remain some weaknesses in the approach. The ex vivo preparations morphologically

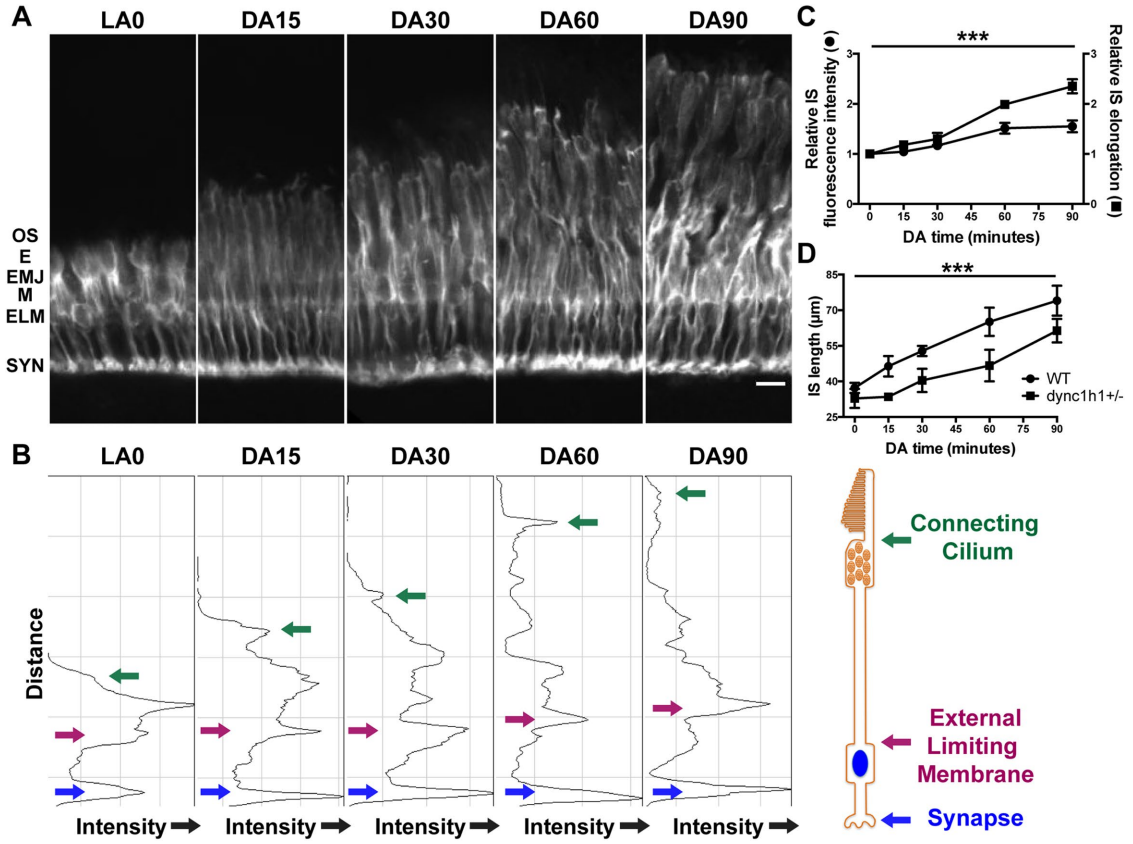

FIGURE 7: In vivo cone myoid elongation is dependent on cytoplasmic dynein-1. (A) Cryosections of adult TαCP:tdEOS-tubulin fish depicting microtubule organization of cone photoreceptors. Of note, light-adapted fish (LA0) have an intense labeling of microtubules at the EMJ, suggesting a concentration of polymerized microtubules prepared for myoid elongation. Following DA for 90 min, cone myoid elongation is observed as a steady, progressive elongation. Scale bar is 10 μm. OS: outer segment; E: ellipsoid; EMJ: ellipsoid–myoid junction; M: myoid; ELM: external limiting membrane; SYN: synapse. (B) Line intensity analysis of the tdEOS-tubulin cones reveals distinct peaks of tdEOS-tubulin signal associated with the synapse, ELM (Supplemental Figure S5), and basal body (Supplemental Figure S6) of the connecting cilium as depicted in the cone model at the right. (C) Using the line intensity analysis, the distance between the peak of tdEOS-tubulin signal at the ELM and connecting cilium was measured at five timepoints of DA ($n = 6$ fish at each timepoint, 30 total cells at each timepoint) to determine rates of IS (including both ellipsoid and myoid) elongation (squares, top line). In addition, the total tdEOS-tubulin signal within the IS (circles, bottom line) is calculated as the area under the curve between the ELM and connecting cilium from the line intensity analysis ($n = 6$ fish at each timepoint) and standardized to the area under the curve for the synapse peak to control for varying levels of transgene expression. IS elongation and tdEOS-tubulin signal are both normalized to 1 for the light-adapted timepoint. Two-way ANOVA was performed to determine significance in the difference between the rate of IS elongation and the increase in tdEOS-tubulin signal within the IS ($p = 0.0006$, shown). There is a significant, but modest, increase in tdEOS-tubulin fluorescence in the IS ($p < 0.0001$) that accompanies an even more dramatic elongation of the inner segment ($p < 0.0001$). Data are depicted as mean ± SEM. (D) A separate experiment investigating rates of in vivo myoid elongation between adult wild-type ($n = 5$ fish at each timepoint, 15 total cells at each timepoint) and *dync1h1*+/– ($n = 5$ fish at each timepoint, 15 total cells at each timepoint) sibling zebrafish. Two-way ANOVA was performed to determine significance in the difference between wild-type and *dync1h1*+/– zebrafish ($p = 0.0002$, shown). Data are depicted as mean ± SEM.

degenerate after ~6 h in culture, prohibiting long-term imaging and analysis of myoid elongation. Further, only 20% of isolated CIS–COS exhibited quantifiable myoid elongation in our experiments, suggesting that isolation irreparably damaged many of the CIS–COS or that our culture conditions were not ideal. Current work focusing on small slices of intact retina with mosaic expression of TαCP:tdEOS-tubulin should provide the benefits of resolving the cytoskeleton of individual photoreceptors with better modeling in vivo myoid elongation.

Additionally, while we have shown in vivo myoid elongation occurs at 0.5 μm/min, the rates of ex vivo myoid elongation in the CIS–COS is approximately half, at 0.2 μm/min. One potential explanation for the decreased rates of myoid elongation ex vivo is due to the lack of sufficient plasma membrane outflow to the myoid. Although plasma membrane from both the cell body and ellipsoid may contribute to the expanding myoid compartment in vivo, the source plasma membrane is limited to solely the ellipsoid and intracellular pools in CIS–COS, potentially restricting overall rates of elongation. Another possible explanation is that cytoplasmic dynenin-1–mediated microtubule shuttling from the ellipsoid into the myoid is only part of the cytoskeletal rearrangement that leads to myoid elongation. In our line intensity analysis,

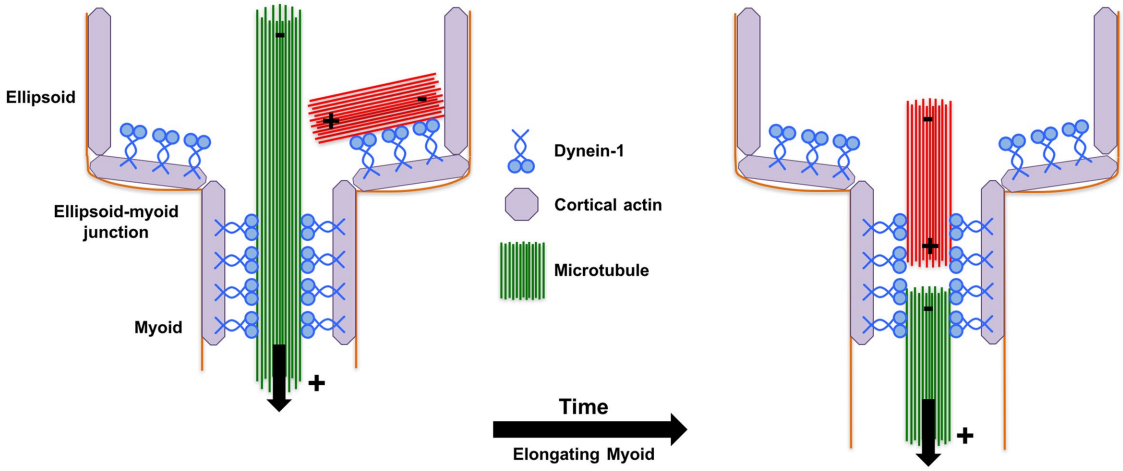

FIGURE 8: Model of cytoplasmic dynein-1–mediated myoid elongation. Myoid elongation involves the shuttling of microtubules from the ellipsoid, through the EMJ, and finally into the extending myoid over time. As depicted, a polymerized, green microtubule is shuttling through the EMJ. Over time, additional polymerized microtubules, such as the red-labeled microtubule, subsequently pass through the EMJ. Within the myoid, there are likely intermicrotubule interactions that bundle microtubules and allow multiple microtubules to move synchronously during the entire time course of myoid elongation. As these microtubules are oriented with their plus ends toward the myoid, and minus ends toward the ellipsoid (Troutt and Burnside, 1988), stationary cytoplasmic dynein-1 complexes anchored around the EMJ could provide the locomotive force necessary for the shuttling of microtubules that is ultimately responsible for myoid elongation. Related to a similar mechanism of cytoplasmic dynein-1 involvement in axon outgrowth (del Castillo *et al.*, 2015), the stationary cytoplasmic dynein-1 complexes could be anchored to cortical actin (Supplemental Figure S7). However, other possibilities for the anchor could be a putative complex bound to the plasma membrane or another cytoskeletal structure.

we observed a small influx of tdEOS-tubulin into the IS (Figure 7C). While this could be explained by diffusion of soluble tdEOS-tubulin into the increased volume of the myoid as it elongates, previous work has shown a small decrease in perinuclear microtubules during myoid elongation (Warren and Burnside, 1978). It is thus possible that there is an additional mechanism for microtubule shuttling from the cell body into the myoid during elongation. Comparable to our cytoplasmic dynein-1 model around the EMJ, stationary kinesin motors around the adherens junctions of the external limiting membrane (Supplemental Figure S5) could function to shuttle microtubules with the minus ends pointed into the elongating myoid. Because CIS–COS do not contain this nuclear compartment, the other portion of the cytoskeletal rearrangement involved in myoid elongation would be missing, leading to the decreased rates of elongation ex vivo compared with in vivo.

However, the myoid that forms from CIS–COS is remarkably comparable to that observed in vivo. The diameter of a myoid from an elongated CIS–COS is ~350 nm (Figures 2 and 3), which is similar to in vivo myoids (Figure S2). Additionally, the average fluorescence intensity of tdEOS-tubulin in the myoid is almost sixfold greater than the fluorescence intensity of microtubules in the ellipsoid (Supplemental Figure S3), suggesting there are several microtubules in the elongating myoid of a CIS–COS, comparable to an elongated myoid in vivo. Although our data does not discount that perinuclear microtubules could still be involved in myoid elongation, we definitively show that the unidirectional movement of microtubules from the ellipsoid to myoid mediated by cytoplasmic dynein-1 is an essential step in this process.

Although we have focused on cone myoid elongation in this work, the contribution of the cytoskeleton to other retinomotor movements remains to be studied. For example, while an anchored cytoplasmic dynein complex may be able to provide the forces for cone myoid elongation, it would be unable to facilitate cone myoid contraction. In support of this, cone myoid contraction is believed to be an actin-dependent, microtubule-independent process (Burnside, 1978). Additionally, both rod myoid elongation and contraction are proposed to be actin dependent and microtubule independent, although microtubules are still present in the rod myoid (O'Connor and Burnside, 1982; Pagh-Roehl *et al.*, 1992). However, given the ease of this established model of tracking movement of subpopulations of tdEOS-tubulin–labeled microtubules, the approach used here could still provide insight into the underlying molecular mechanisms and regulation of the two retinomotor movements in both cone and rod photoreceptors.

Although retinomotor movements are believed to be largely restricted to teleosts and amphibians, the Stiles-Crawford effect suggests that human photoreceptors must be able to align their OS with the incidence path of light to accommodate efficient phototransduction (Stiles and Crawford, 1933). Given the prevalence of cytoplasmic microtubules within the mammalian IS (Woodford and Blanks, 1989), it is possible that a similar mechanism to that proposed here may apply to controlling the orientation of mammalian OS.

MATERIALS AND METHODS

Animal husbandry

Adult zebrafish (*Danio rerio*) on the ZDR genetic background were housed at 28.5°C on a 14-h:10-h light:dark cycle. Embryos were raised at 28.5°C on a 14-h:10-h light:dark cycle. All experiments were approved and conducted in accordance with the Institutional Animal Care and Use Committee of the Medical College of Wisconsin. For all experiments involving animals, male and female animals were randomly assigned to each experimental group. For experiments involving genetic mutants, all zebrafish used were siblings.

Transgenesis

A CMV:tdEOS-tubulin plasmid was received as a gift from Vladimir Gelfand (Northwestern, Evanston, IL; Lu *et al.*, 2013). Using the Gateway system, the tdEOS-tubulin tagged gene was cloned into a new vector flanked with *Tol2* sites and under control of the TαCP promoter (Kennedy *et al.*, 2007), otherwise known as the cone α transducin (gnat2) promoter. The *Tol2* transposon system was used where one-cell zebrafish embryos were injected with 9.2 nl of a mixture containing 25 ng/μl of plasmid and 10 ng/μl of transposase mRNA from an in vitro transcription reaction. Injected embryos were screened at 4 dpf for expression of the construct, and positive embryos were raised to adulthood. Adults were then in-crossed and resultant screening of offspring embryos led to the generation of a stable line of zebrafish expressing TαCP:tdEOS-tubulin. For certain experiments, injected embryos with transient and mosaic expression of TαCP:tdEOS-tubulin were used to better analyze the cytoskeletal structure of individual cones.

CIS–COS isolation

Adult (2 to 6 mo old) zebrafish were dark-adapted overnight and at light onset, were anesthetized in tricaine. Retinas were dissected in a 2:1 mixture of L15 medium (Sigma, St. Louis, MO) and water (hereafter termed L10 medium) and then gently shaken in imaging dishes (MatTek, Ashland, MA) previously coated for 20 min in 0.5 mg/ml peanut lectin (Sigma). Under these conditions, cones break at the myoid and the mitochondria-rich CIS–COS can be cultured for several hours for experimental treatments (Burnside *et al.*, 1993). CIS–COS were allowed to settle for 1 h before imaging at room temperature. For drug treatment experiments, retinas dissected from an individual fish were separated with one retina undergoing drug treatment and the other retina used as a control.

SIM

SIM was performed on a N-SIM (Nikon Instruments, Melville, NY) equipped with an XY Miniscanner (Bruker, Billerica, MA) to allow for focal photoconversion at 405 nm. Images were obtained with a 100× oil-immersion, 1.49-NA objective (Nikon Instruments). NIS-Elements (Nikon Instruments) software was used for image collection.

Confocal microscopy

Confocal microscopy was performed on a C1 Plus-EX3 AOM Confocal System (Nikon Instruments). Images were obtained with a 60× oil-immersion, 1.4-NA objective (Nikon Instruments). Nikon EZ-C1 software (Nikon Instruments) was used for image collection.

Electron microscopy

Enucleated eyes from dark-adapted 4 mo ZDR zebrafish were fixed overnight in 2% glutaraldehyde, 2% tannic acid, and 0.5% saponin in 0.08 M cacodylate buffer (pH 7.4) (Tilney *et al.*, 1973; Fujiwara and Linck, 1982). Eyes were postfixed in 1% osmium tetroxide followed by dehydration in a graded methanol series and infusion with Embed 812 epon (Electron Microscopy Sciences, Hatfield, PA). Sections (70 nm) were collected on 200 Mesh hexagonal grids (Electron Microscopy Sciences), and subsequently stained with uranyl acetate (Electron Microscopy Sciences). Transmission electron microscopy (TEM) imaging was performed on a Hitachi H-600 with an ORCA-100 digital camera (Hamamatsu, Hamamatsu City, Japan).

CIS–COS measurements and analysis

Photoconversion of a 1–2 μm spot was performed on isolated CIS–COS with elongating myoids. Following photoconversion, images were obtained at 5-min intervals. The fluorescence intensity of the photoconverted red signal was measured along the entire length of the myoid. The length of the spot was defined as the distance between the half-intensity points on either end of the photoconverted spot. For each timepoint, the length of the spot was measured and normalized to the initial postconversion measurement ($t = 0$). Additionally, the distance between the base of the ellipsoid (defined as the ellipsoid–myoid junction) and the center of the photoconverted spot was measured at all five timepoints. Myoid elongation was calculated as the change in distance between the center of the photoconverted spot and the base of the ellipsoid across timepoints. For measuring the distance between the photoconverted spot and the tip of the myoid, the center of the photoconverted spot and the far distal tip of the myoid were measured across all timepoints. For frequency of myoid elongation, the CIS–COS exhibiting myoid elongation of 5 μm or greater were counted against the total number of CIS–COS observed. The frequency of myoid elongation was then normalized to the average of the frequency of myoid elongation in control medium. For intensity of the myoid compared with an ellipsoid microtubule, the average intensity of a line through the length of the myoid, the length of an ellipsoid microtubule, and then a background spot within the ellipsoid not containing a polymerized microtubule was calculated with ImageJ. The average intensity of the background spot was subtracted from both the myoid and the ellipsoid microtubule measurements before ratioing the two measurements. For counting the microtubules within the ellipsoid, only filamentous, straight microtubules were counted and standardized to the initial timepoint.

Drug treatments

For nocodazole treatment experiments, L10 medium was supplemented with a final concentration of 3.3 μM nocodazole (Sigma) dissolved in water. The corresponding control had the same volume of water supplemented to the L10 medium. Ciliobrevin D (EMD Millipore, Billerica, MA; Firestone *et al.*, 2012) was used between 10 and 25 μM and dissolved in dimethyl sulfoxide (DMSO). The final concentration of DMSO in all ciliobrevin D–treated CIS–COS was 0.025% DMSO. Corresponding vehicle controls had 0.025% DMSO for all sets of experiments. For wash-out experiments, CIS–COS were cultured in a small volume (300 μl) of either 20 μM ciliobrevin D or 0.025% DMSO for 1 h after isolation. After quantifying the frequency of myoid elongation, a large volume (2500 μl) of L10 medium was added to each imaging dish to significantly dilute the drugs. Latrunculin B (Abcam, Cambridge, MA) was used at 10 μM and dissolved in DMSO. The final concentration of DMSO in all latrunculin B-treated CIS–COS was 0.02% DMSO. Wash-out experiments for latrunculin B were performed as described above. For all drug treatment experiments, retinas dissected from an individual fish were separated with one retina undergoing drug treatment and the other retina used as a control.

Immunofluorescence staining

For cryosection staining of cytoplasmic dynein-1 components, eyes from light-adapted adult (2 mo) zebrafish were enucleated and fixed in 4% paraformaldehyde (PFA) in phosphate-buffered saline (PBS). For cryosection staining of phalloidin, whole 7 dpf embryos that were injected with TαCP:tdEOS-tubulin for mosaic expression were fixed in 4% PFA in PBS. Following fixation, samples were infiltrated with sucrose and embedded in OCT freezing medium before being cut into 12-μm sections and subsequently stained. For ex vivo CIS–COS staining, isolated CIS–COS from TαCP:tdEOS-tubulin fish were fixed in 4% PFA in PBS and subsequently stained.

The Dync1H1 (20928), total Dynein IC (V3), and Dync1I2 (IC2; Vaughan and Vallee, 1995; Vaughan *et al.*, 2001; Whyte *et al.*, 2008) antibodies were gifts from Richard Vallee (Columbia University, New York, NY) and Kevin Vaughan (University of Notre Dame, Notre Dame, IN). Adherens junctions and the actin cytoskeleton were stained with Alexa Fluor 594 phalloidin (Invitrogen, Waltham, MA). Basal bodies were stained with GTU-88, a mouse monoclonal anti-γ-tubulin (Abcam), and rabbit polyclonal anti-centrin1 (C7736; Sigma) antibodies. Secondary antibodies included goat anti-rabbit immunoglobulin G (IgG) Alexa Fluor 594 and goat anti-mouse IgG Alexa Fluor 405 (Invitrogen).

In vivo myoid elongation and line intensity analysis

To measure rates of myoid elongation in vivo, adult (2 mo) zebrafish expressing TαCP:tdEOS-tubulin were dark-adapted at the normal time of dark onset. Zebrafish were then killed at each of five timepoints: light-adapted (LA0), DA15, DA30, DA60, and DA90. For each fish, one eye was enucleated and fixed in 4% PFA in PBS. Samples were then cryoembeded and sectioned as described above. ImageJ was used for subsequent image analysis. For each image, a 110-µm line was drawn from synapse to OS and used to plot the pixel intensity of tdEOS-tubulin along the length. The IS length was calculated as a measure of the distance between a peak associated with the external limiting membrane and a peak associated with the base of the connecting cilium. tdEOS-tubulin signal intensity within the IS was calculated as the area under the curve between these two points and standardized to the area under the curve of the peak associated with the synapse to control for varying levels of expressing of tdEOS-tubulin. For relative IS fluorescence intensity and relative IS elongation, these values were normalized to LA0.

Quantification and statistical analysis

For all experiments involving imaging, quantification was performed on blinded images. For cell-counting experiments involving myoid elongation frequency, isolated CIS–COS were blinded to the analyzer. For all experiments, quantified data are depicted as mean ± standard error of the mean (SEM). For analysis of spot lengths and elongation lengths over time with nocodazole treatment, repeated measures two-way analysis of variance (ANOVA) was performed to determine statistical significance. For analysis of frequency of myoid elongation with nocodazole treatment, an unpaired, two-tailed *t* test was performed to determine statistical significance. For analysis of distances between the spot and the distal tip of the myoid or between the spot and the ellipsoid–myoid junction over time, repeated measures two-way ANOVA was performed to determine statistical significance with a Bonferroni's multiple comparison post hoc analysis performed to determine statistical significance between timepoints for each measurement. For analysis of microtubule number in the ellipsoid between elongating and nonelongating cells, repeated measures two-way ANOVA was performed to determine statistical significance with a Bonferroni's multiple comparison post hoc analysis performed to determine statistical significance between timepoints for each group. For analysis of frequency of myoid elongation with varying doses of ciliobrevin D treatment, a two-way ANOVA was performed to determine statistical significance with a Bonferroni's multiple comparison post hoc analysis performed to determine statistical significance for each specific concentration. For analysis of frequency of myoid elongation with drug washouts, a two-way ANOVA was performed to determine statistical significance with a Bonferroni's multiple comparison post hoc analysis performed to determine statistical significance pre- and postwash. For analysis of frequency of myoid elongation of *dync1h1*+/– CIS–COS, an unpaired, two-tailed *t* test was performed to determine statistical significance. For comparing the relative IS fluorescence intensity to the relative IS elongation, a two-way ANOVA was performed to determine statistical significance. For comparing the rate of IS elongation over time between wild-type and *dync1h1*+/– fish, a two-way ANOVA was performed to determine statistical significance. For all experiments, significance is labeled as $*p \le 0.05$, $**p \le 0.01$, $***p \le 0.001$, $****p \le 0.0001$. Nonsignificant values are unlabeled.

ACKNOWLEDGMENTS

This work was supported by National Eye Institute Research Grants No. R01 EY03222 (J.C.B.) and No. R01 EY014167 (B.A.L.), as well as by a Core Grant for Vision Research (Grant No. P30 EY001931). T.R.L. was supported by a Training Program in Vision Science (T32 EY014537). The funders had no role in study design, data collection and analysis, decision to publish, or preparation of the manuscript.

REFERENCES

Ali MA (1975). Retinomotor responses. In: Vision in Fishes: New Approaches in Research, ed. Ali MA, Boston, MA: Springer US, 313–355.

Atchison DA, Smith G (2006). Optics of the Human Eye, Oxford, UK: Butterworth-Heinemann, 21–29.

Besharse JC, Dunis DA, Burnside B (1982). Effects of cyclic adenosine 3′,5′-monophosphate on photoreceptor disc shedding and retinomotor movement. Inhibition of rod shedding and stimulation of cone elongation. J Gen Physiol 79, 775–790.

Burnside B (1978). Thin (actin) and thick (myosinlike) filaments in cone contraction in the teleost retina. J Cell Biol 78, 227–246.

Burnside B (2001). Light and circadian regulation of retinomotor movement. Prog Brain Res 131, 477–485.

Burnside B, Wang E, Pagh-Roehl K, Rey H (1993). Retinomotor movements in isolated teleost retinal cone inner-outer segment preparations (CIS-COS): effects of light, dark and dopamine. Exp Eye Res 57, 709–722.

Butler R, Wood JD, Landers JA, Cunliffe VT (2010). Genetic and chemical modulation of spastin-dependent axon outgrowth in zebrafish embryos indicates a role for impaired microtubule dynamics in hereditary spastic paraplegia. Dis Model Mech 3, 743–751.

del Castillo U, Winding M, Lu W, Gelfand VI (2015). Interplay between kinesin-1 and cortical dynein during axonal outgrowth and microtubule organization in *Drosophila* neurons. eLife 4, e10140.

Efremov VI, Gluzdikova GM, Mukhachev EV (2007). Development of the model of the cell cycle synchronization in early embryos of *Danio rerio* (Teleostei). Ontogenez 38, 372–379.

Firestone AJ, Weinger JS, Maldonado M, Barlan K, Langston LD, O'Donnell M, Gelfand VI, Kapoor TM, Chen JK (2012). Small-molecule inhibitors of the AAA+ ATPase motor cytoplasmic dynein. Nature 484, 125–129.

Fujiwara K, Linck RW (1982). The use of tannic acid in microtubule research. Methods Cell Biol 24, 217–233.

Gilson CA, Ackland N, Burnside B (1986). Regulation of reactivated elongation in lysed cell models of teleost retinal cones by cAMP and calcium. J Cell Biol 102, 1047–1059.

Hillman DW, Lin D, Burnside B (1995). Evidence for D_4 receptor regulation of retinomotor movement in isolated teleost cone inner-outer segments. J Neurochem 64, 1326–1335.

Hodel C, Neuhauss SC, Biehlmaier O (2006). Time course and development of light adaptation processes in the outer zebrafish retina. Anat Rec A Discov Mol Cell Evol Biol 288, 653–662.

Insinna C, Baye LM, Amsterdam A, Besharse JC, Link BA (2010). Analysis of a zebrafish *dync1h1* mutant reveals multiple functions for cytoplasmic dynein 1 during retinal photoreceptor development. Neural Dev 5, 12.

Jesuthasan S, Stahle U (1997). Dynamic microtubules and specification of the zebrafish embryonic axis. Curr Biol 7, 31–42.

Kennedy BN, Alvarez Y, Brockerhoff SE, Stearns GW, Sapetto-Rebow B, Taylor MR, Hurley JB (2007). Identification of a zebrafish cone photoreceptor-specific promoter and genetic rescue of achromatopsia in the *nof* mutant. Invest Ophthalmol Vis Sci 48, 522–529.

Levinson G, Burnside B (1981). Circadian rhythms in teleost retinomotor movement. A comparison of the effects of circadian rhythm and light condition on cone length. Invest Ophthalmol Vis Sci 20, 294–303.
Liepe BA, Burnside B (1993). Cyclic nucleotide regulation of teleost rod photoreceptor inner segment length. J Gen Physiol 102, 75–98.
Lu W, Fox P, Lakonishok M, Davidson MW, Gelfand VI (2013). Initial neurite outgrowth in *Drosophila* neurons is driven by kinesin-powered microtubule sliding. Curr Biol 23, 1018–1023.
McKinney SA, Murphy CS, Hazelwood KL, Davidson MW, Looger LL (2009). A bright and photostable photoconvertible fluorescent protein. Nat Methods 6, 131–133.
Mendieta-Serrano MA, Schnabel D, Lomeli H, Salas-Vidal E (2013). Cell proliferation patterns in early zebrafish development. Anat Rec (Hoboken) 296, 759–773.
Menger GJ, Koke JR, Cahill GM (2005). Diurnal and circadian retinomotor movements in zebrafish. Vis Neurosci 22, 203–209.
O'Connor P, Burnside B (1982). Elevation of cyclic AMP activates an actin-dependent contraction in teleost retinal rods. J Cell Biol 95, 445–452.
Pagh-Roehl K, Brandenburger J, Wang E, Burnside B (1992). Actin-dependent myoid elongation in teleost rod inner/outer segments occurs in the absence of net actin polymerization. Cell Motil Cytoskeleton 21, 235–251.
Pagh-Roehl K, Han E, Burnside B (1993). Identification of cyclic nucleotide-regulated phosphoproteins, including phosducin, in motile rod inner-outer segments of teleosts. Exp Eye Res 57, 679–691.
Pagh-Roehl K, Lin D, Su L, Burnside B (1995). Phosducin and PP33 are *in vivo* targets of PKA and type 1 or 2A phosphatases, regulators of cell elongation in teleost rod inner-outer segments. J Neurosci 15, 6475–6488.
Potter C, Zhu W, Razafsky D, Ruzycki P, Kolesnikov AV, Doggett T, Kefalov VJ, Betleja E, Mahjoub MR, Hodzic D (2017). Multiple isoforms of nesprin1 are integral components of ciliary rootlets. Curr Biol 27, 2014–2022.
Rao AN, Patil A, Black MM, Craig EM, Myers KA, Yeung HT, Baas PW (2017). Cytoplasmic dynein transports axonal microtubules in a polarity-sorting manner. Cell Rep 19, 2210–2219.
Rey HL, Burnside B (1999). Adenosine stimulates cone photoreceptor myoid elongation via an adenosine A2-like receptor. J Neurochem 72, 2345–2355.
Rodieck RW (1998). The First Steps in Seeing, Sunderland, MA: Sinauer Associates.
Scherer J, Yi J, Vallee RB (2014). PKA-dependent dynein switching from lysosomes to adenovirus: a novel form of host-virus competition. J Cell Biol 205, 163–177.
Spira AW, Milman GE (1979). The structure and distribution of the cross-striated fibril and associated membranes in guinea pig photoreceptors. Am J Anat 155, 319–337.
Stiles WS, Crawford BH (1933). The luminous efficiency of rays entering the eye pupil at different points. Proc R Soc Lond B Biol Sci 112, 428–450.
Taylor SS (1989). cAMP-dependent protein kinase. Model for an enzyme family. J Biol Chem 264, 8443–8446.
Tilney LG, Bryan J, Bush DJ, Fujiwara K, Mooseker MS, Murphy DB, Snyder DH (1973). Microtubules: evidence for 13 protofilaments. J Cell Biol 59, 267–275.
Troutt LL, Burnside B (1988). Microtubule polarity and distribution in teleost photoreceptors. J Neurosci 8, 2371–2380.
Troutt LL, Wang E, Pagh-Roehl K, Burnside B (1990). Microtubule nucleation and organization in teleost photoreceptors: microtubule recovery after elimination by cold. J Neurocytol 19, 213–223.
Vaughan PS, Leszyk JD, Vaughan KT (2001). Cytoplasmic dynein intermediate chain phosphorylation regulates binding to dynactin. J Biol Chem 276, 26171–26179.
Vaughan KT, Vallee RB (1995). Cytoplasmic dynein binds dynactin through a direct interaction between the intermediate chains and $p150^{Glued}$. J Cell Biol 131, 1507–1516.
Warren RH, Burnside B (1978). Microtubules in cone myoid elongation in the teleost retina. J Cell Biol 78, 247–259.
Welsh JH, Osborn CM (1937). Diurnal changes in the retina of the catfish, *ameiurus nebulosus*. J Comp Neurol 66, 349–359.
Whyte J, Bader JR, Tauhata SB, Raycroft M, Hornick J, Pfister KK, Lane WS, Chan GK, Hinchcliffe EH, Vaughan PS, Vaughan KT (2008). Phosphorylation regulates targeting of cytoplasmic dynein to kinetochores during mitosis. J Cell Biol 183, 819–834.
Woodford BJ, Blanks JC (1989). Localization of actin and tubulin in developing and adult mammalian photoreceptors. Cell Tissue Res 256, 495–505.
Yang J, Gao J, Adamian M, Wen XH, Pawlyk B, Zhang L, Sanderson MJ, Zuo J, Makino CL, Li T (2005). The ciliary rootlet maintains long-term stability of sensory cilia. Mol Cell Biol 25, 4129–4137.
Zhang X, Lei K, Yuan X, Wu X, Zhuang Y, Xu T, Xu R, Han M (2009). SUN1/2 and Syne/Nesprin-1/2 complexes connect centrosome to the nucleus during neurogenesis and neuronal migration in mice. Neuron 64, 173–187.